Site-specific specimen preparation for SIMS analysis of radioactive samples

Junliang Liu[1], Kexue Li[1, 2]*, Sergio Lozano-Perez[1], Chris R. M. Grovenor[1]

[1]Department of Materials, University of Oxford, Parks Road, United Kingdom

[2]Department of Materials, University of Manchester, Oxford Road, Manchester, UK.

*Corresponding author: kexue.li@manchester.ac.uk

Abstract

Secondary Ion Mass Spectrometry is an important technique for the study of the composition of a wide range of materials because of the exceptionally high sensitivity that allows the study of trace elements and the ability to distinguish isotopes that can be used as markers for reactions and transport processes. However, when studying nuclear materials, it is often necessary to analyse highly radioactive samples, and only rather few SIMS facilities are available in active environments. In this paper, we present a methodology using focussed ion beam milling to prepare samples from radioactive specimens that are sufficiently large to undertake SIMS mapping experiments over microstructurally-significant regions, but with overall activities small enough to be readily transported and analysed by a SIMS instrument in a normal laboratory environment. Radioactive samples prepared using this methodology can also be used for correlative SIMS analysis with other analytical microscopies. SIMS results showing the distributions of deuterium in oxides on in-reactor corroded zirconium alloys are presented to demonstrate the potential of this sample preparation technique.

Keywords: High-resolution secondary ion mass spectrometry (SIMS); Focused ion beam (FIB); Sample preparation; Zirconium alloys; Hydrogen Pickup; Nuclear materials.

1. Introduction

Secondary ion mass spectrometry (SIMS) analysis has been used for many years to evaluate and improve the performance of materials used in nuclear reactors (Portier et al. 2007, Li et al. 2020). Compared to the most commonly used analytical tool, electron probe microanalysis (EPMA), SIMS offers the capability to detect even the lightest elements and to distinguish between isotopes. As reviewed in (Portier et al. 2007), SIMS can be used for a wide range of studies in nuclear materials, including precise isotope ratio measurements and the analysis of the migration of fission products in spent fuels (Gerlach et al. 2006, Desgranges et al. 2009), the long-term degradation behaviour of nuclear waste disposal materials (Valle et al. 2010), stress corrosion cracking in reactor steels (Lozano-Perez et al. 2008), aqueous corrosion and hydrogen pick-up in fuel cladding (McIntyre et al. 1991, Yardley et al. 2013, Li et al. 2019), and the characterisation of plasma-facing materials in fusion devices (Koivuranta et al. 2014). There are several previous reports of the value of depth profiling and 3D characterization of zirconium alloys for nuclear applications by SIMS. For example the study of hydrogen or deuterium diffusion through oxides on Zr alloys (McIntyre et al. 1990, Mcintyre et al. 1991, Elmoselhi 1995, Tupin et al. 2017), the incorporation of cations like Li Na and K into zirconium oxide (Jeong et al. 1999), and the study of second phase particles (SPPs) (Hatano et al. 1996, Baur et al. 2000, Bossis et al. 2000). Recently, we have shown that high-resolution SIMS analysis of oxidised zirconium alloys using a CAMECA NanoSIMS 50 instrument enables the 3D characterisation of deuterium distributions (Li et al. 2019, Liu et al. 2020).

However, to allow the analysis of highly active nuclear components, complex modifications are required to SIMS instruments to protect both the electronic components and the operators from radiation exposure and contamination. To our knowledge, only a limited number of fully shielded SIMS instruments are available for the analysis of ex-reactor nuclear materials, e.g. an A-DIDA-SIMS at Paul Scherrer Institute (PSI) (Bart et al. 1981) and Cameca IMS 6f at CEA Cadarache (Rasser et al. 2003) and in the Institute for Transuranium Elements (ITU) (Brémier et al. 2006).

Zirconium alloys have been used as the fuel cladding in many types of nuclear reactors for many years, and hydrogen pickup (HPU) is one of the major degradation mechanisms limiting its in-service lifetime (Motta et al. 2019). In our recent work (Li et al. 2019, Liu et al. 2020) we

have used high resolution SIMS analysis to reveal the 3-dimensional (3D) distribution of deuterium in oxides formed on Zr alloys in autoclaves, and proposed that interconnected nano-pores in the oxide layers can serve as the preferential transportation pathways for hydrogen from the external cathode to the underlying metal. Because of the limited availability of SIMS instruments that can be used to study highly active samples, only few attempts have been made to carry out similar characterisation of the distribution of hydrogenic species in oxides formed under in-pile conditions (McIntyre et al. 1991, Ramasubramanian et al. 2000, Tupin et al. 2017), and more data is needed to develop more robust mechanisms for in-reactor HPU.

Focused ion beam (FIB) milling has been widely applied to the preparation of transmission electron microscopy (TEM) and atom probe tomography (APT) samples (Giannuzzi 2004, Lozano-Perez 2008, Li et al. 2018, Chen et al. 2020). In this paper, we present a methodology using FIB milling to prepare samples from nuclear fuel cladding zirconium alloys that are designed specifically for correlative SEM/EDX and SIMS analysis. By applying this methodology to a small piece of bulk fuel cladding material (3 mm × 3 mm × 1 mm) with a rather modest measured activity of ~1.8 x 10^4 Bq, we estimate the activity of the final specimen is reduced to an unmeasurable value < 6.5 x 10^{-3} Bq in the FIB lift-out sample, and this can then be analysed in a non-nuclear instrument. This methodology has been used to prepare radioactive samples for SIMS analysis in our recent work (Liu et al. 2020), in which we have measured the deuterium diffusion coefficients in zirconium oxides formed in-reactor, and provided direct evidence showing that irradiation can increase the rate of key mechanisms controlling transport of deuterium through the oxide layers on Zr alloys. More results comparing hydrogen and deuterium analysis in Zr alloys from bulk and FIB lift-out samples can be found in (Li et al. 2019, Liu et al. 2020).

2. Materials

The Zr-2.5Nb (wt%) alloy used in this study was provided by our collaborators in Canadian Nuclear Laboratories (CNL). Typical microstructures of this alloy and its corrosion and HPU performance have been described in previous papers (Hovington et al. 2009, Nordin et al. 2012). Samples were tested in the Halden reactor and exposed to neutron irradiation in a

water chemistry of D_2O, 250°C and 10 MPa, LiOD, pH=10.5. These corroded Zr-2.5Nb samples were provided in small coupons (3 mm × 3 mm × 1 mm) for FIB specimen preparation. More information on the in-reactor corroded sample is summarised in Table 1. Using the methodologies introduced below, the FIB lift-out SIMS specimen has a volume of ~25 × 25 × 5 μm^3, and based on the measurement of the original bulk sample our estimate of the activity of the SIMS specimen is < 6.5×10^{-3} Bq, too low to be measured. As a comparison, the activity of a banana is about 4 Bq because of the ^{40}K it contains (Zagatto et al. 2008). This estimate shows that materials of much higher activity could be prepared by the same lift-out process for SIMS analysis without reaching a level of activity that would cause practical problems in a normal laboratory environment.

The natural isotopic abundance of deuterium (^2H) is only 1.15×10^{-4}, so we can be confident that nearly all the signal at 2 Daltons originates from deuterium originating from the corrosion process trapped in the sample microstructure. Other hydrogenic species (^1H and H_2) can be contaminants from both the sample surface and the high vacuum chamber (although the background pressure is $\sim 1.3 \times 10^{-11}$ kPa). However taking advantage of the excellent mass resolving power of the Cameca NanoSIMS instrument, clear separation of the $^2H^-$ and $^1H_2^-$ signals around 2 Daltons can be achieved using a mass resolving power of about 1300 (Li et al. 2019), and so unwanted contributions to a $^2H^-$ signal from H_2^- can be ignored under our typical analysis conditions.

Table 1 Information of the in-reactor corroded Zr-2.5Nb sample used in this study.

Sample	Corrosion time (days)	Oxide thickness (μm)	Deuterium content* (ppm)	Sample dimensions (mm^3)	Sample activity (Bq)
Zr-2.5Nb (wt%)	190	1.2	9.2	3 × 3 × 1	1.8×10^4

*****The values of deuterium content are measured using hot vacuum extraction mass spectrometry (HVEMS) (Bickel et al. 2002).

3. Sample preparation

To map the distribution of deuterium in the oxide layer on Zr alloys using SIMS, two analysis geometries, in-depth and cross-sectional analysis, have been explored in our previous study (Li et al. 2019). In the in-depth analysis, Figure 1 (a), the primary ion beam is rastered

over a selected region of the surface oxide, and the in-depth elemental distribution can be obtained simply by recording sequential SIMS maps as the surface is gradually eroded away by the incident ion beam probe. In the cross-sectional analysis, Figure 1 (b), samples are mounted with the oxide/metal interface exposing to the incident ion beam, and SIMS mapping is carried from the cross-sectional surface covering both the oxide layer and metal matrix. For cross-sectional analysis, the samples need to be ground using silicon carbide paper down to 4000 grit, and subsequently polished over several hours using water-diluted colloidal silica (Yardley et al. 2013, Li et al. 2019) to generate a flat surface. The mechanical polishing procedures may result in artefacts and redistribution of deuterium, and during cross-sectional SIMS analysis we have observed that the top edge of the oxide is sputtered away much faster than the bulk oxide (Li et al. 2019) due to the well-known edge effect in sputter analysis (Magee et al. 1982) leading to the generation of obvious surface topography. Moreover, on a cross-sectional sample, the oxide layer is very thin (~ 1 µm in this study), giving small effective analysis area, and because of its insulating nature it charges much more than the neighbouring Zr metal matrix. This can cause dramatic changes in signal intensity when the primary ion beam sputters regions of different conductivity and work function during cross-sectional SIMS mapping. These issues can be avoided by using the in-depth analysis which can provide large effective analysis area with negligible disturbance from sample preparation, and have uniform charging at the bottom of the SIMS analysis crater which lies for most of the analysis wholly in either the oxide or the metal matrix. In summary, to characterise the deuterium distribution in active samples of oxidised zirconium using a non-nuclear instrument, a sample preparation methodology will be needed to; 1) lift out small volume samples with reduced activities and 2) allow in-depth SIMS analysis.

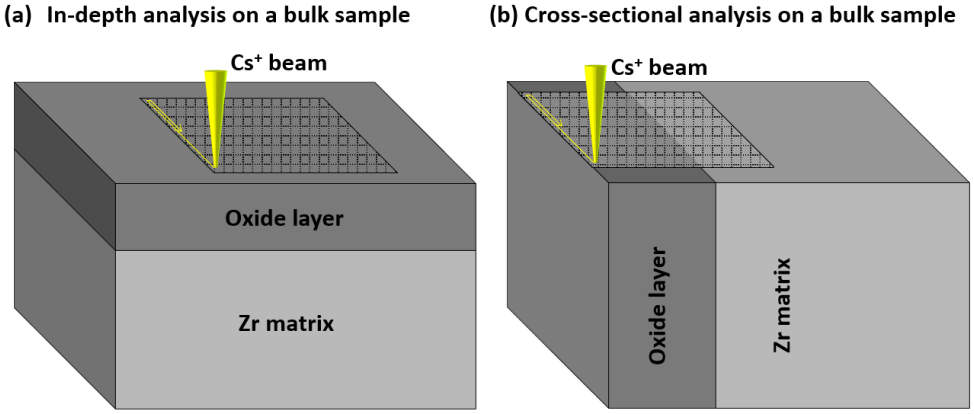

Figure 1 Schematic of SIMS analysis geometries on bulk samples (a) in-depth analysis and (b) cross-sectional analysis.

Here we described a methodology for preparing site-specific, small-volume specimens by FIB for SIMS analysis. This methodology was first tested on non-radioactive samples on a Zeiss Crossbeam 540 FIB/SEM system, and step-by-step instructions for preparation of a specimen suitable for SIMS analysis developed during these trial sessions (as shown in Figure 2). A cross-sectional polished sample was used during the test sessions and the dark grey oxide layer can be seen in Figure 2 (a). Once this protocol was established, samples were prepared following similar protocols from the in-reactor specimens using the Thermal Fisher Helios NanoLab 600i FIB/SEM system installed in facilities for the handling of radioactive materials in the Materials Research Facility (http://www.ccfe.ac.uk/mrf.aspx) at the Culham Centre for Fusion Energy (CCFE). The key stages in this protocol are:

(1) *Loading sample:* Since we decided that in-depth analysis is the best way to study of the deuterium distribution in zirconium oxides, samples that have as small a volume as possible need to be prepared with the surface oxide retained on the top surface. To meet this requirement, the bulk sample is first loaded into the FIB/SEM chamber with the cross-section of the metal/oxide interface exposed to the electron beam. In Figure 2 (a) the zirconium matrix, oxide and the sample holder are labelled. The in-reactor corroded samples are not mechanically polished to reduce the need for processing of radioactive samples, and so the oxide layer is not easily visible, and in that case an estimation of the oxide thickness should be known before preparation to ensure the correct positioning of milling patterns in the following procedures.

(2) *Trench milling*: The stage is tilted to 54° (52° for a Thermal Fisher Helios FIB/SEM) with the ion beam incidence direction normal to the cross-sectional sample surface. After selecting the region of interest (ROI) for a lift-out specimen, a trench is then milled adjacent to the selected region using the regular cross-section milling pattern, for which the ion beam mills a staircase-shaped pattern towards the defined pattern margin that is closer to the oxide layer . The starting pattern for trench 1 is milled at 30 kV and 65 nA, and is placed 15 µm away from the oxide/metal interface to leave enough space for the beam tails. The ion beam size and its heat-affected zone as a function of beam current have been reported in (Ishitani et al. 1995, Bassim et al. 2014), which can be used to evaluate and adjust the spacing between the milling pattern and the liftout region. The width of the pattern for milling trench 1 is set as 30 µm, which might result in the final trench larger than 35 µm in the end due to the beam tail effect,

especially when working with large ion beam currents, and the depth of cut is set as 30 µm which will determine the effective analysis area for the SIMS mapping. To ensure that SIMS analysis right down into the metal matrix will be possible, a layer of metal matrix of ~3 µm is left between the final milling pattern (at 30 kV and 7 nA) for trench 1 and the oxide/metal interface. This sublayer of metal matrix will also help to reduce any artefacts induced during FIB milling like elemental redistribution in the region of interest (the top oxide layer in this study) caused by beam heating. However, to ensure the bottom of the lamella can be completely released in procedure (3), we suggest the total thickness of the lamella (oxide layer + sublayer of metal matrix in this study) should be less than 8 µm. The SEM image in Figure 2 (b) taken at 0° stage tilt shows an example of the completed milling of trench 1. This step of trench milling takes about 40-50 min. Note that when we mount the bulk sample, a gap is left between the sample surface and the sample holder, Figure 2 (a), and by mounting the sample in this strategy, only one trench will be required. If the region of interest is not at the sample surface, then a second trench must be milled from the other side of the ROI following the similar strategy to that described above.

(3) *Under-cut:* To perform the under-cut process, the stage is tilted back to horizontal. Three milling patterns are positioned at the edges of the ROI to mill the channels. Typically the width of the patterns for milling the channels is 3 µm, which might result in channels larger than 4 µm in the end due to beam tails adjacent to the pattern site. A “bridge” linking part was left at one of the top corners, which supports the lamella until it is cut free from the bulk sample in the procedure (4). The current used for under-cut is 7 nA at 30 kV. For a lamella with 5 µm thickness (oxide layer thickness + the sublayer of metal matrix), the milling depth needs to be larger than 6.2 µm (5 µm/cos36°). To remove any redeposition, we suggest this under-cut procedure needs to be repeated 3-5 times. Note that it is very important to ensure the channels are cut thoroughly in order to lift out the lamella successfully in procedure (4). As the volume of sputtered material is rather large, it is important to check from different angles (by tilting the stage) whether there is material redeposition between the lamella and the bulk sample, especially at the corner regions at the bottom of the trench 1. The thicker the lamella is, the more likely the sputtered materials will redeposit and reconnect the lamella to the bulk sample, and the more effort will be needed for under-cut milling. For a 5 µm thick

specimen, this under-cut procedure takes about 30 mins. The SEM and FIB images in Figure 2 (c) show an example of the lamellar surrounded by finished channels.

(4) *Lift out:* The fourth step is to lift out the lamella from the bulk sample. The stage is tilted to horizontal (0° tilt) and the micro-manipulator needle is then inserted and carefully operated to touch the lamella at the corner opposite to the "bridge" linking part. We suggest that the Gas Injection system (GIS) for Pt deposition should be inserted before the manipulator needle is too close to the lamella (> 20 µm) to avoid any damage to the lamella caused by the possible vibration induced during inserting the GIS. A Pt layer (5 µm × 5 µm × 2 µm) is deposited using an ion beam with 0.7 nA current and the "rectangle" pattern function to weld the lamella to the micro-manipulator needle. As the lamella for the SIMS characterisation is of relatively large volume, this Pt layer is therefore thicker and larger than that used for conventional TEM samples to provide sufficient connecting strength. Once the lamella is welded to the manipulator needle, the remaining 'bridge' linking part is milled away at a beam current of 3 nA at 30 kV. The lamella is then entirely detached from the bulk sample and can be readily lifted out by moving the micro-manipulator. The FIB images in Figures 2 (d and e) show an example of the lift-out process. This step takes about 30 min.

(5) *Mounting the lamella to the FIB lift-out grid:* After being lifted out from the bulk sample, the lamella needs to be mounted to a grid so that it can be transferred for SIMS analysis. A standard FIB lift-out TEM half-grid (Omniprobe lift-out grid) is used in this step. When mounting the grids, care should be taken that the fingers of the grids face up to the incident electron beam so that the lamella can be welded on the top surface of the grid. Once the grid is at the working distance, the micro-manipulator is then inserted. SEM- and FIB-view imaging from two directions are used to monitor the movement of the manipulator and ensure the lamella reaches the top surface of the grid. As before, the GIS for Pt deposition need to be inserted before the manipulator needle is too close to the middle bar. Once the lamella touches the top surface of the grid, a layer of Pt (30 µm × 5 µm × 2 µm is deposited at 1.5 nA and 30 kV using the "rectangle" pattern function to weld one edge of the lamella to the grid. After the lamella has been welded to the grid, the micro-manipulator needle can be fully detached using a milling current of 3 nA at 30 kV. Note that to increase the welding strength, the Pt deposition process is repeated on every side of the lamella after retracting

the micromanipulator. An example of a welded lamella is shown in Figure 2 (g and i). This step takes about 60 mins.

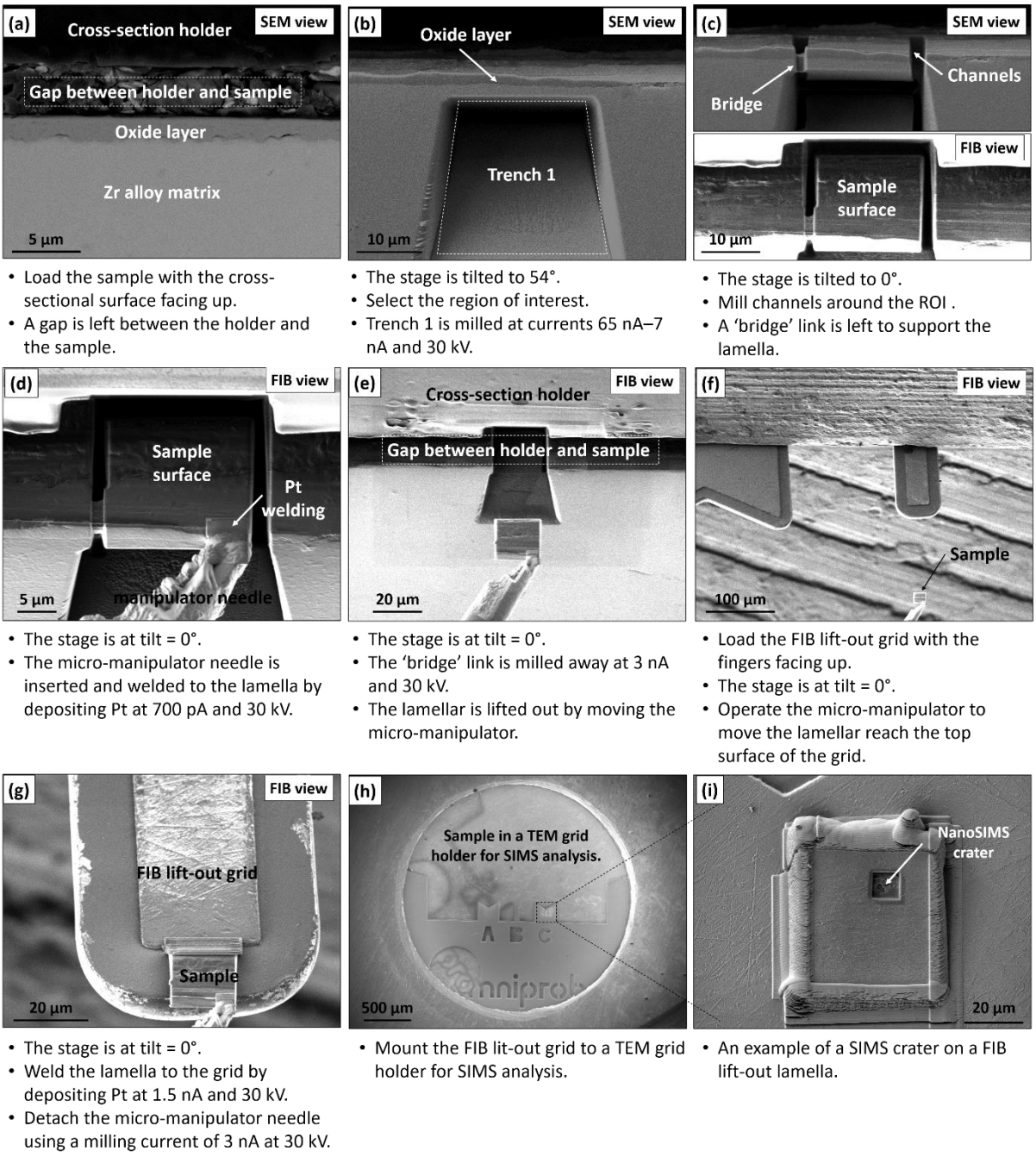

- Load the sample with the cross-sectional surface facing up.
- A gap is left between the holder and the sample.

- The stage is tilted to 54°.
- Select the region of interest.
- Trench 1 is milled at currents 65 nA–7 nA and 30 kV.

- The stage is tilted to 0°.
- Mill channels around the ROI .
- A 'bridge' link is left to support the lamella.

- The stage is at tilt = 0°.
- The micro-manipulator needle is inserted and welded to the lamella by depositing Pt at 700 pA and 30 kV.

- The stage is at tilt = 0°.
- The 'bridge' link is milled away at 3 nA and 30 kV.
- The lamellar is lifted out by moving the micro-manipulator.

- Load the FIB lift-out grid with the fingers facing up.
- The stage is at tilt = 0°.
- Operate the micro-manipulator to move the lamellar reach the top surface of the grid.

- The stage is at tilt = 0°.
- Weld the lamella to the grid by depositing Pt at 1.5 nA and 30 kV.
- Detach the micro-manipulator needle using a milling current of 3 nA at 30 kV.

- Mount the FIB lit-out grid to a TEM grid holder for SIMS analysis.

- An example of a SIMS crater on a FIB lift-out lamella.

Figure 2 SEM and FIB images showing the processes during FIB lift-out specimen preparation for SIMS analysis. (a) Sample loading, (b) Trench milling, (c) Under cut, (d-e) Lift out, (f-g) Mounting the lamella to the FIB lift-out grid, (h) A FIB lift-out grid mounted in a TEM grid holder for SIMS analysis and (i) An SEM image showing a finished lift-out sample after SIMS analysis. The key settings are indicated below each step.

(6) *Transferring the FIB lift-out specimen:* After the GIS retraction and chamber venting, the FIB lift-out grid is mounted to a specially designed TEM grid holder, which can then be

used for in-depth SIMS analysis. Figure 3 shows a schematic diagram of the TEM grid holder, on which the grid as well as the specimen top surface will face upwards. This TEM grid holder enables the mounting of up to three FIB lift-out grids, and can fit into a 10 mm aperture in a conventional Cameca NanoSIMS 'Biology' holder. Before insertion into the NanoSIMS, we suggest coating the FIB-lift-out grids with 5 nm of platinum to avoid charging from the insulating oxide layer. An example of the crater created in the surface oxide layer by in-depth SIMS analysis is shown in Figure 2 (i).

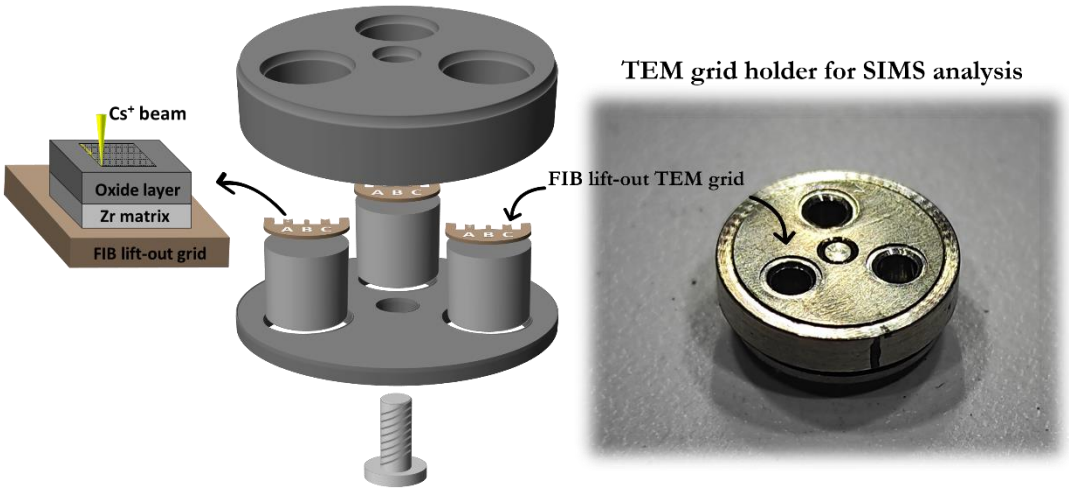

Figure 3 A TEM grid holder for SIMS analysis. This TEM grid holder can fit into a 10 mm aperture in a NanoSIMS 'Biology' holder.

4. SIMS and SEM/EDX analysis

High-resolution SIMS analyses were performed using a CAMECA NanoSIMS 50 with a 16 keV Cs^+ primary ion beam. The primary aperture was inserted (D1 = 2, 300 µm) resulting in a primary ion beam with beam current of 2.5 pA and approximate diameter 150 - 200 nm. Ion maps 10 µm × 10 µm were collected simultaneously for $^1H^-$ and $^2H^-$ ion signals together with the secondary electron (SE) signal produced during the sputtering process, with a pixel time of 0.5 ms (7.74×10^3 Cs^+ ions/pixels) at a resolution of 256 × 256 pixels with an image dose of 5.07×10^{14} Cs^+ ions/cm^2. These scans were repeated up to 10000 times (~19 hrs) from the same region with total Cs^+ ion dose of 5.07×10^{18} Cs^+ ions/cm^2, giving a set of stacked 2-dimensional (2D) images of the distributions of each signal, and sputtering to a total depth up to 3 µm below the sample surface. The sputtering rate in the oxide is about 0.22 (nm × μm^2)/pA/s, which is very close to previous values of 0.19 to 0.20 (nm × μm^2)/pA/s reported for zirconium oxide (Li et al. 2019). During SIMS analysis, data is collected from the sputtered

bottom of the crater, and if any serious surface topography is developed this will cause a problem with the creation of accurate depth profiles and 3D data reconstruction. However, our previous results show that the average roughness of the crater bottom in similar fine grained zirconium oxide samples is only 64 ± 25 nm for the same raster size 10 × 10 µm (Li et al. 2019). This value is small enough compared to a typical sputtered depth of ~3 µm that we can be sure that the depth profiles and 3D reconstructions do not include severe geometric artefacts from crater roughness. ImageJ with the OpenMIMS plugin (Poczatek et al. 2012) was then used for data analysis and plotting depth profiles.

The samples welded using the suggested methodology are strong enough to transport for correlative analysis using different microscopies. To demonstrate the correlative analysis, scanning electron microscopy (SEM) and energy dispersive X-ray (EDX) analysis was carried out at the bottom of SIMS craters in a Zeiss Crossbeam 540 instrument using a 5 kV accelerating voltage to reduce beam spreading and degradation of spatial resolution. The EDX information depth in ZrO_2 at 5 kV accelerating voltage was estimated using a CASINO V2.48 Monte-Carlo Simulation program to be ~ 80 nm (Hovington et al. 1997), and the effective information depth for the in-depth SIMS analysis can be estimated to be the thickness of the layer sputtered to produce each image, ~0.18 nm.

5. Results and discussion

5.1. Deuterium distribution in in-reactor corroded Zr-2.5Nb alloy

The in-depth SIMS analysis can generate a series of 2D maps which can then be processed and enable viewing the distributions of elements from different directions. Figure 4 shows a set of cross-sectional SIMS images extracted from a typical in-depth analysis dataset. The different charging processes on the surface oxide layer and metal matrix lead to a dramatic difference in secondary electron signal when the primary ion beam is incident on these different materials. As a result, the location of the oxide/metal interface can be easily recongnised from contrast variations in the SE image, Figure 4 (a). The $^{1}H^{-}$ and $^{2}H^{-}$ signals are both high in the top 300 nm of the oxide layer, Figure 4 (b and c) ,where a high density of interconnected nano-porosity and fine cracks are observed in similar samples (Ni et al. 2010) that can act as possible trapping sites (Couet et al. 2019, Hu et al. 2019), and then drop to a

much lower level deeper into the oxide. The $^{1}H^{-}$ signal can also be seen to have a peak closer to the oxide surface than the $^{2}H^{-}$ signal, as also shown in the depth profiles in Figure 6. This makes sense in a sample corroded exclusively in heavy water if the hydrogen (^{1}H) signal comes from environmental contamination, and is thus expected mostly at the sample surface. The $^{2}H^{-}$ signal penetrates much more deeply into the oxide layer, Figures 4 (c) and 5, with a decrease in intensity ~0.5 µm from the oxide/metal interface which corresponds the location of the compact inner oxide layer (Couet et al. 2019, Hu et al. 2019). The high intensity of the $^{1}H^{-}$ signal from regions of the metal matrix, Figures 4 (b) and 5, we suppose to be an artefact of sample preparation. The ion beam can stimulate hydrogen contaminants in the chamber to adsorb onto the reactive Zr surface, and hydrogen at 50 °C can diffuse ~10 µm in 1 h in zirconium (Carpenter et al. 1995). Once absorbed on the reactive surface, the local temperature increase caused by beam heating (Ishitani et al. 1995) can then encourage hydrogen diffusion into the bulk sample, and perhaps the formation of hydrides (Hanlon et al. 2019). These beam heating-induced artefacts thus need to be taken into consideration when applying this specimen preparation methodology for SIMS analysis, and could be reduced to some extent by leaving a thicker sublayer between the FIB milling trench and the FIB lift-out region (but at the cost of increasing the FIB milling time).

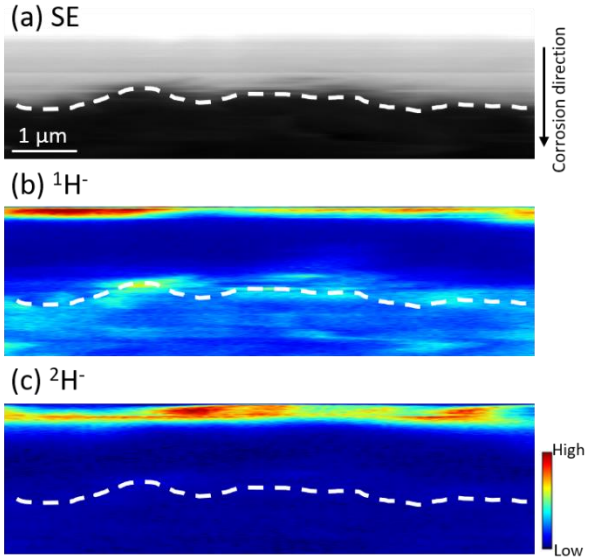

Figure 4 Cross-sectional view of (a) SE, (b) $^{1}H^{-}$ and (c) $^{2}H^{-}$ images extracted from an in-depth SIMS dataset from an in-reactor corroded Zr-2.5Nb sample. In the SE map the oxide shows bright contrast and the metal matrix dark. The white dashed lines indicate the positions of the oxide/metal interface.

The in-depth SIMS data can be used to generate 1-dimesional (1D) depth profiles of the kind more commonly reported for HPU studies (McIntyre et al. 1991, Abolhassani et al. 2015, Tupin et al. 2017). Typical depth profiles for $^{1}H^{-}$ and $^{2}H^{-}$ signals through the oxide into the metal matrix are shown in Figure 5. Depth profiles showing similar distributions of hydrogen and deuterium in an in-reactor corroded Zr alloy have been reported by McIntyre et. al. (McIntyre et al. 1991) which gives us confidence that our sample preparation processes are not seriously modifying the deuterium distribution. We thus propose that this methodology can be used for the study of a wider range of ex-reactor samples in non-active SIMS facilities. We have also calculated the diffusion coefficient of deuterium in our sample by fitting the $^{2}H^{-}$ depth profile shown in Figure 5 with the appropriated solution to Fick's 2nd law as described previously (Tupin et al. 2015, Li et al. 2019). The diffusion coefficient in the oxide in this sample corroded at 250°C is $5.9 \pm 1.5 \times 10^{-22}$ m^2/s. A similar material corroded under the same water chemistry but at 325°C shows, as expected, a significant higher value of $5.2 \pm 3.0 \times 10^{-21}$ m^2/s (Liu et al. 2020). The measurement of deuterium diffusion coefficients in oxides on a wider range of Zr alloys, water chemistry and temperatures can be found in (Liu et al. 2020).

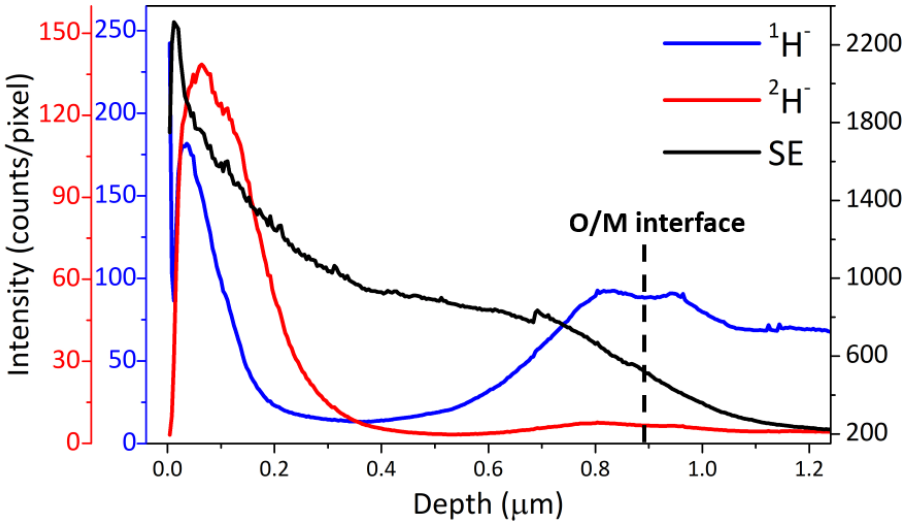

Figure 5 SIMS depth profiles of $^{1}H^{-}$ and $^{2}H^{-}$ signals extracted from an in-depth SIMS dataset from an in-reactor corroded Zr-2.5Nb sample.

5.2. Correlative SEM/EDX and SIMS analysis

Correlating SIMS imaging with other microscopies (SEM, EDX and TEM) has been used to generate key microstructural and microchemical information at different length scales to help

understand the mechanisms controlling the degradation of physical and mechanical properties (Eswara et al. 2019). . The sample preparation methodology introduced in this paper enables the safe and easy transportation of radioactive samples, and also provides the potential for correlating SIMS with other analytical microscopies. Figure 6 shows an example of correlative SIMS mapping, high-resolution SEM imaging and EDX elemental analysis on a FIB lift-out SIMS specimen from a similar in-reactor Zr-2.5Nb sample corroded at 325°C. We detected significantly reduced $^{2}H^{-}$ counts from the regions of the SE images that showed brighter contrast, Figure 6 (a and b). In order to be sure of the nature of these bright regions in the SIMS SE image, we carried out EDX analysis of the same area to show that the bright, D-poor regions are rich in Nb, Figure 6 (d and e). The SEM image in Figure 6 (c) provided structural information, showing the SIMS crater surface is quite flat, as described above. These results show that the Nb-enriched secondary phases in the Zr-2.5Nb alloy are not preferential trapping sites for deuterium, which is important for understanding its diffusion processes through the oxide layers. More details on the diffusion of hydrogenic species through zirconium oxides can be found in (Couet et al. 2019, Hu et al. 2019).

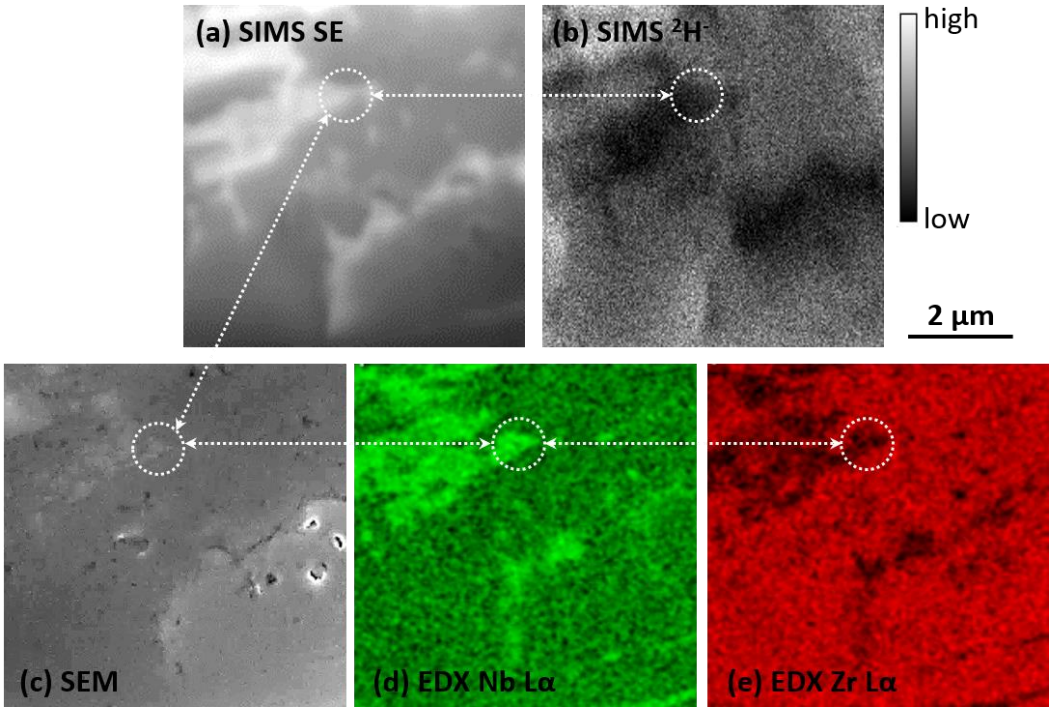

Figure 6 Correlative SIMS mapping. (a) SE and (b) $^{2}H^{-}$ maps in the oxide on a Zr-2.5Nb sample corroded at 350°C under in-reactor conditions, with (c) SEM and (d, e) EDX characterisation. Images (a and b) are integrated SE and $^{2}H^{-}$ signals from the last 30 SIMS slices (~5 nm) before the EDX analysis. The dashed lines indicate the same region in all the images. Images (a), (b) and (d) are reprinted from Fig. 11 of (Liu et al. 2020), Copyright (2020), with permission from Elsevier.

6. Conclusions

- A methodology using FIB to prepare site-specific, small volume radioactive specimens for SIMS analysis is presented in this paper. These specimens with much reduced activities can then be analysed by a SIMS instrument without complex nuclear modifications or being sited in an active environments. Radioactive samples prepared using this methodology can also be used for correlating SIMS mapping with other analytical microscopies like SEM and EDX. This methodology can also be applied to prepare other hazardous materials for SIMS analysis.
- The distribution of deuterium in the in-reactor corroded Zr alloys has been mapped using in-depth analysis in the NanoSIMS. The deuterium diffusion coefficient calculated using the $^{2}H^{-}$ depth profile acquired from the oxide on an in-reactor Zr-2.5Nb sample corroded at 250 °C is $5.9 \pm 1.5 \times 10^{-22}$ m^2/s.

Acknowledgements

The authors acknowledge the contribution made to this work by their collaborators from the MUZIC project and Dr. Heidi Nordin from Canadian Nuclear Laboratories providing zirconium samples. This study is funded by the UK Engineering and Physical Sciences Research Council (EPSRC) under grant EP/M018237/1. Some of the work on radioactive samples was done using UKAEA's Materials Research Facility funded by the UK's National Nuclear User Facility and Henry Royce Institute initiative. EPSRC grant (EP/N010868/1) is acknowledged for funding the Zeiss Crossbeam used in this research. Junliang Liu is grateful for support from EPSRC grant (EP/P001645/1).

References

Abolhassani, S., Bart, G., Bertsch, J., et al. (2015). Corrosion and hydrogen uptake in zirconium claddings irradiated in light water reactors. Zirconium in the Nuclear Industry: 17th International Symposium, *ASTM International*, 540-573.

Bart, G., Aerne, T., Flückiger, U., et al. (1981) Modification of a secondary ion mass spectrometer to allow the examination of highly radioactive specimens. *Nucl Instrum Methods*. **180**, 109-116.

Bassim, N., Scott, K.& Giannuzzi, L. A. (2014) Recent advances in focused ion beam technology and applications. *MRS Bulletin*. **39**, 317-325.

Baur, K., Garzarolli, F., Ruhmann, H., et al. (2000). electrochemical examinations in 350°c water with respect to the mechanism of corrosion-hydrogen pickup. Zirconium in the Nuclear Industry: 12th International Symposium, *ASTM International*, 836-852.

Bickel, G. A., Green, L. W., James, M. W. D., et al. (2002) The determination of hydrogen and deuterium in Zr–2.5Nb material by hot vacuum extraction mass spectrometry. *J Nucl Mater*. **306**, 21-29.

Bossis, P., Leliegrave, et al. (2000). Multi-scale characterization of the metal-oxide interface of zirconium alloys, Zirconium in the Nuclear Industry: 12th International Symposium, *ASTM International*, 918-945.

Brémier, S., Hasnaoui, R., Portier, S., et al. (2006) Installation of a shielded SIMS for the analysis of irradiated nuclear fuels. *Microchim Acta*. **155**, 113-120.

Carpenter, G. J. C., Jackman, J. A., McCaffrey, J. P., et al. (1995) In situ hydride formation in zirconium and titanium during ion milling. *Microsc Microanal*. **1**, 175-184.

Chen, Y.-S., Lu, H.Liang, J., et al. (2020) Observation of hydrogen trapping at dislocations, grain boundaries, and precipitates. *Science*. **367**, 171-175.

Couet, A., Borrel, L., Liu, J., et al. (2019) An integrated modeling and experimental approach to study hydrogen pickup mechanism in zirconium alloys. *Corros Sci*, **159**, 108134.

Desgranges, L., Pasquet, B., Valot, C., et al. (2009) SIMS characterisation of actinide isotopes in irradiated nuclear fuel. *J Nucl Mater*. **385**, 99-102.

Elmoselhi, M. (1995) Hydrogen uptake by oxidized zirconium alloys. *J Alloy Compd*. **231**, 716-721.

Eswara, S., Pshenova, A., Yedra, L., et al. (2019) Correlative microscopy combining transmission electron microscopy and secondary ion mass spectrometry: A general review on the state-of-the-art, recent developments, and prospects. *Appl Phys Rev*. **6**, 021312.

Gerlach, D. C., Cliff, J. B., Hurley, D. E., et al. (2006) Secondary ionization mass spectrometric analysis of impurity element isotope ratios in nuclear reactor materials. *Appl Surf Sci*. **252**, 7041-7044.

Giannuzzi, L. A. (2004). Introduction to focused ion beams: instrumentation, theory, techniques and practice, Springer Science & Business Media.

Hanlon, S., Persaud, S., Long, F., et al. (2019) A solution to FIB induced artefact hydrides in Zr alloys. *J Nucl Mater*. **515**, 122-134.

Hatano, Y., Isobe, K., Hitaka, R., et al. (1996) Role of intermetallic precipitates in hydrogen uptake of Zircaloy-2. *J Nucl Sci Technol*. **33**, 944-949.

Hovington, P., Drouin, D.& Gauvin, R. (1997) CASINO: A new Monte Carlo code in C language for electron beam interaction—Part I: Description of the program. *Scanning*. **19**, 1-14.

Hovington, P., Pinard, P. T., Lagacé, M., et al. (2009) Towards a more comprehensive microstructural analysis of Zr–2.5Nb pressure tubing using image analysis and electron backscattered diffraction (EBSD). *J Nucl Mater*. **393**, 162-174.

Hu, J., Liu, J., Lozano-Perez, S., et al. (2019) Hydrogen pickup during oxidation in aqueous environments: The role of nano-pores and nano-pipes in zirconium oxide films. *Acta Mater*. **180**, 105-115.

Ishitani, T.& Kaga, H. (1995) Calculation of local temperature rise in focused-ion-beam sample preparation. *J Electron Microsc*. **44**, 331-336.

Jeong, Y. H., Kim, K. H.& Baek, J. H. (1999) Cation incorporation into zirconium oxide in LiOH, NaOH, and KOH solutions. *J Nucl Mater*. **275**, 221-224.

Koivuranta, S., Likonen, J., Hakola, A., et al. (2014) Post-mortem measurements of fuel retention at JET. *Phys Scripta*. **T159**, 014052.
Li, C.Habler, G., Baldwin, L. C., et al. (2018) An improved FIB sample preparation technique for site-specific plan-view specimens: A new cutting geometry. *Ultramicroscopy*. **184**, 310-317.
Li, K., Aarholt, T., Liu, J., et al. (2019) 3D-characterization of deuterium distributions in zirconium oxide scale using high-resolution SIMS. *Appl Surf Sci*. **464**, 311-320.
Li, K., Liu, J., Grovenor, C. R., et al. (2020) NanoSIMS imaging and analysis in materials science. *Annu Rev Anal Chem*. **13**, 273-292.
Liu, J., Li, K., Sayers, J., et al. (2020) Characterisation of deuterium distributions in corroded zirconium alloys using high-resolution SIMS imaging. *Acta Mater*. **200**, 581-596.
Lozano-Perez, S. (2008) A guide on FIB preparation of samples containing stress corrosion crack tips for TEM and atom-probe analysis. *Micron*. **39**, 320-328.
Lozano-Perez, S., Schröder, M., Yamada, T., et al. (2008) Using NanoSIMS to map trace elements in stainless steels from nuclear reactors. *Appl Surf Sci*. **255**, 1541-1543.
Magee, C. W.& Honig, R. E. (1982) Depth profiling by SIMS—depth resolution, dynamic range and sensitivity. *Surf Interface Anal*. **4**, 35-41.
McIntyre, N., Weisener, C., Davidson, R., et al. (1990) Analysis of zirconium–niobium pressure tube surfaces for hydrogen using secondary ion mass spectrometry (SIMS). *Surf Interface Anal*. **15**, 591-597.
Mcintyre, N. S., Davidson, R. D., Weisener, C. G., et al. (1991) Sims studies of hydrogen diffusion through oxides on Zr-Nb alloy. *Surf Interface Anal*. **17**, 757-763.
McIntyre, N. S., Weisener, C. G., Davidson, R. D., et al. (1991) Analysis of Zr-Nb fuel channel surfaces for hydrogen and other elements using Secondary Ion Mass Spectrometry (SIMS). *J Nucl Mater*. **178**, 80-92.
Motta, A. T., Capolungo, L., Chen, L.-Q., et al. (2019) Hydrogen in zirconium alloys: A review. *J Nucl Mater*. **518**, 440-460.
Ni, N., Lozano-Perez, S., Jenkins, M. L., et al. (2010) Porosity in oxides on zirconium fuel cladding alloys, and its importance in controlling oxidation rates. *Scripta Mater*. **62**, 564-567.
Nordin, H., Elliot, A.& Bergin, S. (2012). High temperature aqueous corrosion and deuterium uptake of coupons prepared from the front and back ends of Zr-2.5 Nb pressure tubes, Zirconium in the Nuclear Industry: 16th International Symposium, *ASTM International*, 373-398.
Poczatek, C.,Kaufman, Z.& Lechene, C. (2012) "OpenMIMS ImageJ Plugin Guide." OpenMIMS ImageJ Plugin Guide.
Portier, S., Brémier, S.& Walker, C. T. (2007) Secondary ion mass spectrometry of irradiated nuclear fuel and cladding: An overview. *Int J Mass Spectrom*. **263**, 113-126.
Ramasubramanian, N., Perovic, V.& Leger, M. (2000). Hydrogen transport in the oxide and hydrogen pickup by the metal during out-and in-reactor corrosion of Zr-2.5Nb pressure tube material. Zirconium in the Nuclear Industry: 12th International Symposium, *ASTM International*, 853-876.
Rasser, B., Desgranges, L.& Pasquet, B. (2003) A new shielded SIMS instrument for analysis of highly radioactive materials. *Appl Surf Sci*. **203-204**, 673-678.
Tupin, M., Bisor, C., Bossis, P., et al. (2015) Mechanism of corrosion of zirconium hydride and impact of precipitated hydrides on the Zircaloy-4 corrosion behaviour. *Corro Sci*. **98**, 478-493.
Tupin, M., Martin, F., Bisor, C., et al. (2017) Hydrogen diffusion process in the oxides formed on zirconium alloys during corrosion in pressurized water reactor conditions. *Corro Sci*. **116**, 1-13.
Valle, N., Verney-Carron, A., Sterpenich, J., et al. (2010) Elemental and isotopic (^{29}Si and ^{18}O) tracing of glass alteration mechanisms. *Geochim Cosmochim Acta*. **74**, 3412-3431.
Yardley, S. S., Moore, K. L., Ni, N., et al. (2013) An investigation of the oxidation behaviour of zirconium alloys using isotopic tracers and high resolution SIMS. *J Nucl Mater*. **443**, 436-443.
Zagatto, V. A. B., Medina, N. H., Okuno, E., et al. (2008) Natural Radioactivity in Bananas. *AIP Conference Proceedings*. **1034**, 264-268.